Ibn Al-Haitham Journal for Pure and Applied Sciences
Journal homepage: jih.uobaghdad.edu.iq
PISSN: 1609-4042, EISSN: 2521-3407
IHJPAS. 2025, 38(2)

Fabrication and Study Structure and Optical Properties of $Cu_{0.75}Zn_{0.25}S$ Thin Film

Ali J. Soud[1] and Bushra K.H. Al-Maiyaly[2*]
[1,2]Department of Physics, College of Education for Pure Science (Ibn Al-Haitham), University of Baghdad, Baghdad, Iraq.
*Corresponding Author.

Received: 30 May 2024 Accepted: 10 September 2024 Published: 20 April 2025
doi.org/10.30526/38.2.4022

Abstract

Thin films (CuxZn1-xS) with x = 0.75 nano crystallized were deposited from the alloy on glass substrates in a vacuum ~ 2×10^{-5} mbar by thermal evaporation technique with 450±20 nm thickness. The effects of annealed temperature (deposits, 423, 523, and 623) K for one hour on the structure, morphology, and optical properties of Copper Zinc Sulfide (CZS) films were investigated. The structural properties of Cu0.75Zn0.25S films were examined using the X-ray diffraction (XRD) technique as a function of annealed temperatures. XRD presented the Cu0.75Zn0.25S films as polycrystalline in the environment by a mixed hexagonal structure of CuS-ZnS, preferred orientation along the (201) plane, and crystallite size varying from 8.41-23.28 nm with annealing temperature. Atomic force microscopy (AFM) analysis was used to investigate the morphological properties of Cu0.75Zn0.25S films; the grain size of these films varies with annealing temperature in the range of (58.39 to 139.42) nm with uniform distribution. The influences of annealing temperature on the optical characterization of Cu0.75Zn0.25S thin film were examined using UV-Vis absorption spectroscopy. Direct band gap values of Cu0.75Zn0.25S films are gained from optical absorption measurements with a range (2.3-1.8) eV as a function of annealing temperature. From the results obtained above, it appears to us that the temperature is the most suitable for practical applications, which directed that Cu0.75Zn0.25S thin film is suitable for solar cell applications.
Keywords: CZS, Annealing temperature, Thin films, X-ray diffraction, AFM, Thermal evaporation.

1. Introduction

CuZnS alloys are considered to have common structures of (ZnS) and (CuS), and due to the high absorptivity of these materials, they are used in the application of solar cells and photodetectors (1). The three elements, copper, zinc, and sulfur are non-toxic and easy to obtain due to their abundance in the Earth's crust and their cheap price. In addition to their electrical and optical advantages, they are among the materials recommended for use in solar cells (2, 3). Chalcogenide semiconductors, including (CuS), have simple hexagonal crystal structures with lattice measurements, a = 3.79 Å and c = 16.36 Å (4) ZnS was an n-type semiconductor with energy gaps of around (~3.65 eV) (5). while CuS was a p-type semiconductor and had an energy gap of (1.63-1.87 eV) (6). CuS and ZnS are a mixed structure of two chalcogenide metal films, and samples with high copper content are used as an absorbent layer in optoelectronics and photovoltaic applications. Samples with low copper content are used as window/insulating layers for solar cells (7, 8). The ternary compound alloy will be either n- or p-type and will have a wide energy gap (9,10). ZnS semiconductor is known to absorb UV radiation. 4% of practically all sunlight limits (11). For these important reasons, ZnS semiconductors are synthesized by thin band gap energy semiconductors such as CuS. In addition, CuS is more vulnerable to photo corrosion, this suggests protection across large band gap semiconductors (12). PN junctions were created, which are used in the semiconductors CuS (p-type) and ZnS (n-type) and have the advantage of increasing the lifetime of electrons in earlier recombinants. CuS/ZnS samples are utilized for photocatalytic ordering (13, 14). There are different techniques used by researchers to prepare CuZnS films for example chemically immersion deposits (8,15), pulse laser depositions (16), electrochemical deposition (17), photo chemical depositions (18,19), sol-gel technique (20) spray pyrolysis (3,22,23).and Successive ionic layer absorption (SILAR)(24). In this research, crystalline $Cu_{0.75}Zn_{0.25}S$ thin films have been synthesized by thermal evaporated technique, that influences of annealed temperature (423,523, then 623) K on CZS characterization have been investigated for photo voltaic request.

2. Materials and Methods

The ternary alloy (CZS) was formed from the elements copper and zinc, besides sulfide. The three elements were then mixed and placed in a quartz tube under pressure (3 * 10-4 mbar). The process was done. The tube was placed in an electric oven (1300 K) for more than six hours, at a temperature higher than the melted temperatures for CuS and ZnS, then cooled progressively. The three elements are of high purity (99.99%) in a ratio of 0.75:0.25:1. The physical method was used to prepare thin films by changing the weight ratio of the elements that make up the alloy (0.75:0.25:1)by thermal evaporation using (E 306). Before the deposition process began, using an ultrasonic bath with acetone, ethanol, and deionized water, the substrates were cleaned sequentially. Then, it was deposited in a glass substrate at room temperature with a thickness of 450±20 nanometers before being vacuum annealed at temperatures (423, 523, and 623) K in 60 minutes, where the morphological, structural, and optical properties were studied. XRD technique was used to characterize the structure of all films prepare used CuKα radiation greatest 2Θ from 20° to 80 °. Bragg's law is utilized to consider interplanar spacing (d) of the Miller index (hkl) (25, 26).

$$2d\sin\theta = n\lambda \tag{1}$$

The crystalline size (C.S) of films was valued by utilizing Scherer's Prescription (27,28).

$$C.S = \frac{0.94\lambda}{\beta COS\theta} \tag{2}$$

Where λ: XRD wavelength, β: FWHM of the peaks, and θ: Bragg's angle. The dislocations density (δ) and Micro strain (Ɛ) were estimated by using the equations (3 and 4) respectively (29.30):

$$\delta = \frac{1}{(C.S)2} \tag{3}$$

$$\varepsilon = \frac{BCOS\theta}{4} \tag{4}$$

The morphology of the CZS film surface was examined by using AFM. The transmit and absorb spectrum was recorded to diversity (400-1100) nm to characterize optical properties for all films prepared. The optical energy gap of $Cu_{0.75}Zn_{0.25}S$ thin films before and after annealing was calculated by using Tauc's equation: (31,32).

$$(\alpha h\nu) = D\,(h\nu - E_g)^n \tag{5}$$

hν: the incident photons energy, D: is constant, n: is a number related to the type transition, and α: the absorption coefficient was predicted since absorbance (A) using the equation (33, 34)

$$\alpha = \frac{2.303A}{t} \quad (6)$$

Where t: is film thickens.

Optical constant values like refractive index (n) and extinction coefficient (K) were estimated by using equations (7, 8) respectively (35, 36):

$$n = \{[4R / (R-1)]-K^2\}^{1/2} - [(R+1) / (R-1)] \quad (7)$$

$$K = \frac{\alpha\lambda}{4\pi} \quad (8)$$

Where (R) is reflectance that is intended through (36):

$$R = 1-T-A \quad (9)$$

The loss tangent was estimated by using the equations (29):

$$\tan\delta = \varepsilon i / \varepsilon r \quad (10)$$

Where (**ε_r, ε_i**)**:** the real and imaginary parts of the dielectric constant which are calculated from the equations below (7, 37):

$$\varepsilon_r = n^2-K^2 \quad (11)$$

$$\varepsilon_i = 2nK \quad (12)$$

3. Results and Discussion

The crystalline structure of the prepared film was studied, and **Figure 1** shows the XRD pattern of $Cu_{0.75}Zn_{0.25}S$ with different annealing temperatures. All the films prepared before and after annealing had a polycrystal structure through lower crystallinity, hexagonal structures, and a mixed phase of CuS and ZnS. Comparison with the obtained XRD decorations shows that these shapes match the standard XRD reference patterns ZnS (JCPDS: 65-0309) and CuS (JCPDS: 06-0464). Since we do not have standard reference XRD patterns for the ternary CZS compound, the results are in very reasonable agreement with the JCPDS data. The entire film was diffracted at angle 2 (29.6737 °, 29.9 °, 29.7969 °, and 29.7818 °) earlier and then later annealed to see the corresponding (102) levels. In the figure, no distinct peaks appeared for the Cu, Zn, or S elements. The secondary peaks in the XRD pattern indicate the phase of ZnS and CuS, and the obtained results are consistent with the JCPDS data. After the annealing process, the peak positions change marginally. The intensity of the peaks increases, and the size of the crystals becomes larger after annealing. This suggests that the reduction of defects and regularity strengthens the crystalline films (28).

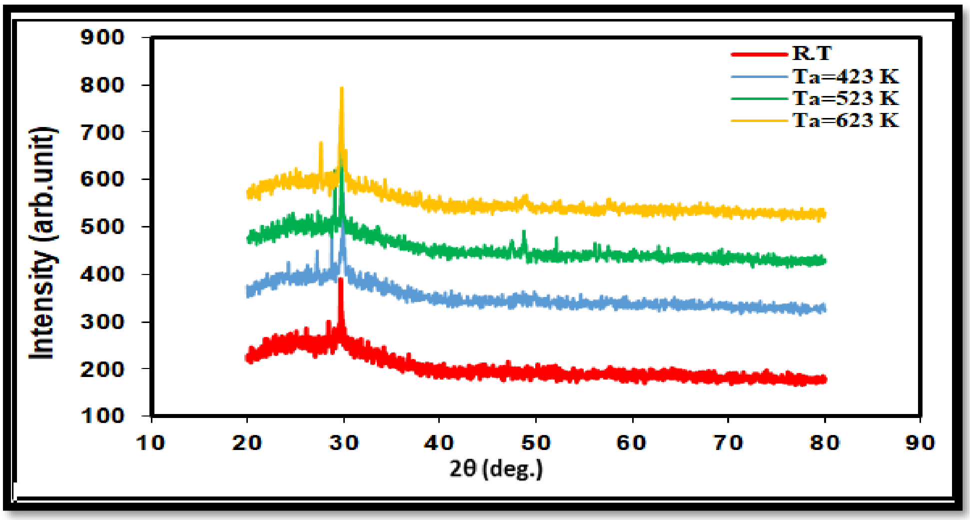

Figure 1. XRD of $Cu_{0.75}Zn_{0.25}S$ thin films at R.T and diverse annealed temperature.

From **Table 1** the calculation values show the density of dislocations (δ), microstrain (Ɛ), and crystallite size (C.S.) for Cu $_{0.75}$ Zn $_{0.25}$ S films. It appears that the value of the size of the nanocrystals increases with increasing annealing temperatures and the values of dislocation density and micro strain decrease after the annealing process. The reason is due to the improvement of the crystalline structure of the films in addition to the decrease in defects. It is also clear from the values in the table of the films (Cu $_{0.75}$ Zn $_{0.25}$ S) annealed at 623 K for one hour have a lower dislocation density, microstrain, and a higher crystalline size compared to other films. This can be attributed to the decrease in the full width at half maximum (FWHM) of the main peak, which ultimately leads to an increase in crystallinity. The size of these films (37). In addition to the observation of the dissimilarity in dislocated density, partial stress is inversely correlated with crystal size, a result that aligns with (21).

Table 1. Structural limitations aimed at Cu $_{0.75}$ Zn $_{0.25}$ S thin film.

T_a (K)	d_{exp} (Å)	$2\theta_{exp}$ (deg.)	(hkl)	FWHM (deg.)	C.S (nm)	$\delta*10^{16}$ (lines/m^2)	$\varepsilon*10^{-3}$
R.T	3.00819	29.6737	102	1.02	8.419517	1.4106707	8.419517
423	2.97783	29.9	102	0.7667	11.20702	7.961957	11.20702
523	2.99603	29.7969	102	0.706	12.16765	6.7544	12.16765
623	3.0001	29.7818	102	0.3689	23.2856	1.844273	23.2856

Through AFM analysis, the effect of annealing temperature on the surface appearance of Cu $_{0.75}$ Zn $_{0.25}$ S thin films with a thickness of (450 nm) was studied at room temperature and next annealed by (423,523,623) K. The AFM images clearly illustrate the gradual dispersion of grains in CZS thin films at varying annealing temperatures. **Figure 2** displays uniform grain surface morphology. As you can see in **Table 2**, the surface roughness values go up with the annealing temperature. They go from 0.953 nm for CZS thin films made at room temperature to 5.05 nm for CZS thin films annealed at 673 K. The surface morphology results presented in **Table 2** indicate an increase in the average grain size from 58.39 nm to 139.42 nm after annealing, which aligns with the X-ray results. The root mean square (RMS) of roughness increases with increasing annealing temperature. All parameters were increased and then annealed, and then the samples annealed at 623 K had higher values. The performance was attributable to the enhancement of the films structurally and the increased movement of atoms. All parameters were increased and then annealed, and then the samples annealed at 623 K had higher values. The performance was attributed to the structural enhancement of the films and the increased movement of atoms, which led to the rearrangement and accumulation of molecules. And increases in the surface roughness of the film, which may play a good role in the performance of thin films for the photovoltaic cells. XRD results showed that the explanations were mostly correct, and there was also an increase in the film's surface roughness, which may be a good thing for the performance of thin films in photovoltaic cells. The explanations were in decent agreement with the XRD consequences, besides reference (37).

Table 2. Roughness average, grain size, and Root mean square of $Cu_{0.75}Zn_{0.25}S$ thin film.

T_a (K)	Grain size (nm)	Roughness average (nm)	Root mean square
R.T	58.39	0.953	1.31
423	81.14	1.67	2.1
523	88.52	2.4	2.74
623	139.42	5.05	7.07

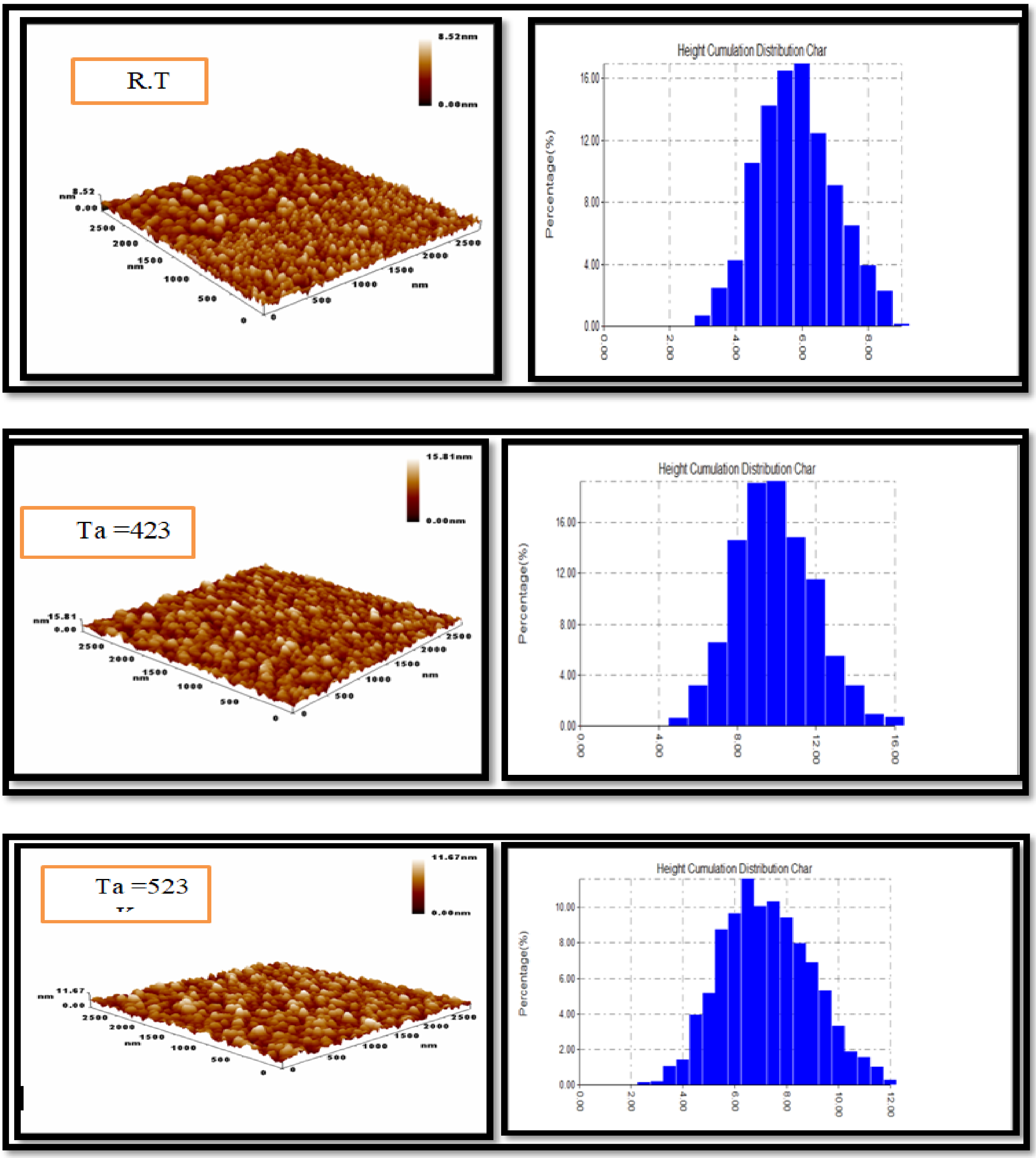

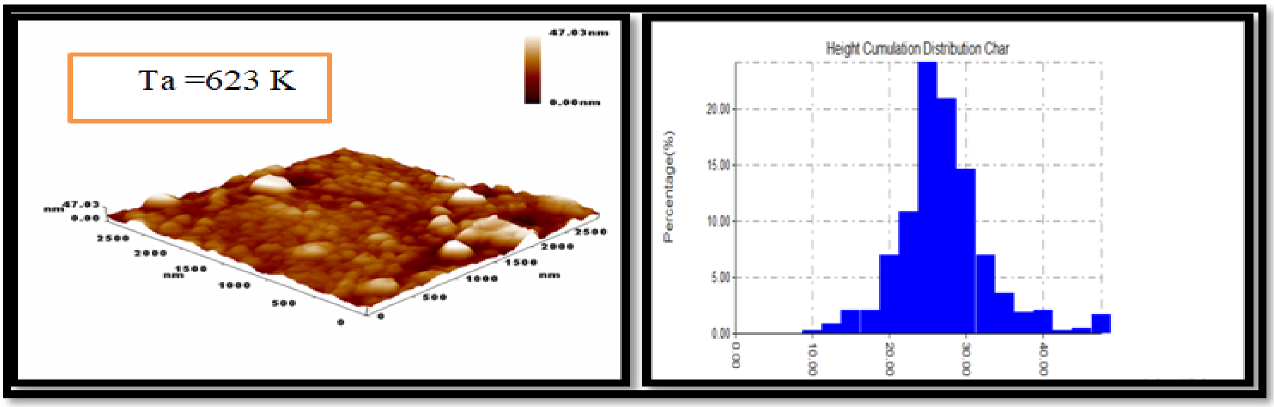

Figure 2. AFM descriptions of $Cu_{0.75}Zn_{0.25}S$ films for diverse annealed temperature.

It is clear to us from **Figure 3** that the optical absorption spectra of Cu $_{0.75}$ Zn $_{0.25}$ S thin film were on wavelength variety (400-1000) nm at room temperature, besides once annealed by (423,523,623) K for 60 minutes. The absorbance values decrease with increasing wavelength, while they increase with cumulative annealing temperature. After annealing, this behavior shows that the optical transmittance values have gone down. These values depend a lot on the crystal structure, chemical composite, surface morphology, and film thickness. Increasing the annealing temperature may result in the size growth of crystallites, leading to reduced optical scattering, which is consistent with the AFM and XRD data. From this figure, the sample annealed at 623 K will have a high absorption value of approximately 80%, and all samples show high absorption in the visible region, which makes these films preferred materials for photovoltaic requests, and the behavior is consistent per studied (40, 7). The absorption coefficient of all films prepared evaluated from equation (6) was found to be ($\alpha > 10^4$ cm^{-1}) which means the allowed direct transition is promising to occur. Also notice that after annealing the absorption coefficient values increase, as publicized on **Figure 3** on behalf of similar details indication earlier.

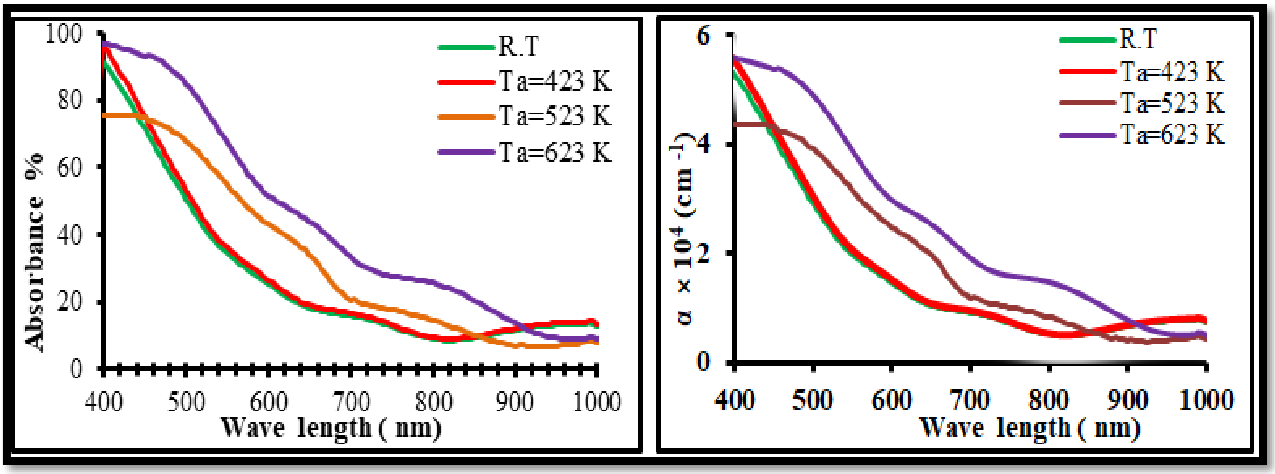

Figure 3. Absorbance and absorption coefficients of $Cu_{0.75}Zn_{0.25}S$ thin films versus wavelength before and after annealing.

The optical energy gap of $Cu_{0.75}Zn_{0.25}S$ thin films was calculated from the plot of $(\alpha h\nu)^2$ compared to hν using Tauc's equation as shown in **Figure 4**. This figure shows the optical energy gap reductions from (2.3 to 1.8) eV through cumulative annealed temperature shifted to lower photon energy. The variant in the optical band gap values may be correlated to the variation in crystallite size and grain boundaries; these values correspond to solar cell application and are in good agreement with (3, 7).

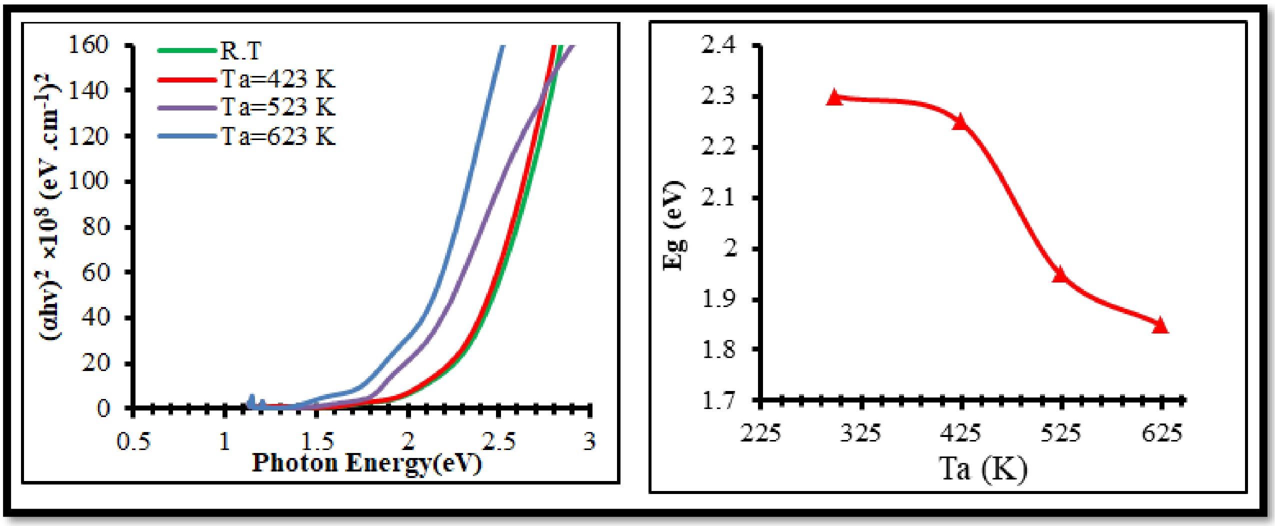

Figure 4. Disparity $(\alpha h\nu)^2$ through photon energy besides optical energy gap for $Cu_{0.75}Zn_{0.25}S$ thin films before and after annealing.

Figure 5 demonstrates that the refractive index (n) values for Cu0.75Zn0.25S thin films varied with wavelength, indicating annealed temperatures, which can be attributed to differences in the film's structural features. **Figure 5** demonstrates how variations in the film's structural features cause the refractive index (n) values to fluctuate with the wavelength of the Cu0.75Zn0.25S thin films, especially during annealed temperatures. Changes in preparation conditions and technology lead to behavioral changes in the refractive index, and several factors, including the type of material and the crystal structure, influence its value. Additionally, the roughness coefficient of the surface of the prepared film influences the refractive index values.

It also demonstrates that all films exhibit peak-to-length movement. Figure 6 illustrates the less wave variation of extinction coefficient (k) values for the Cu0.75Zn0.25S thin film on R.T., which was then annealed at different temperatures. This figure illustrates a similar behavior of the absorption coefficient, with values increasing after annealing, as the extinction coefficient values primarily depend on the arrangement of the absorption coefficient values.

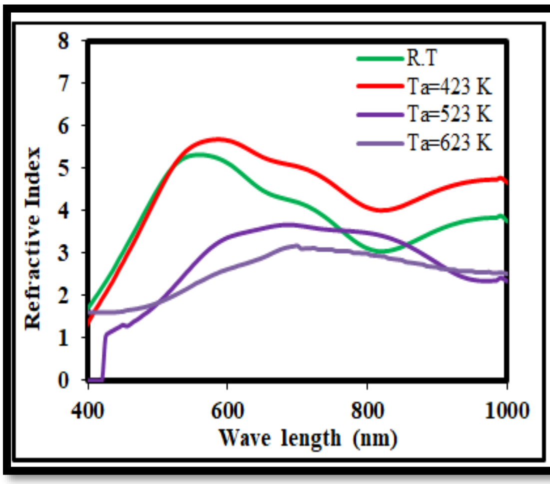

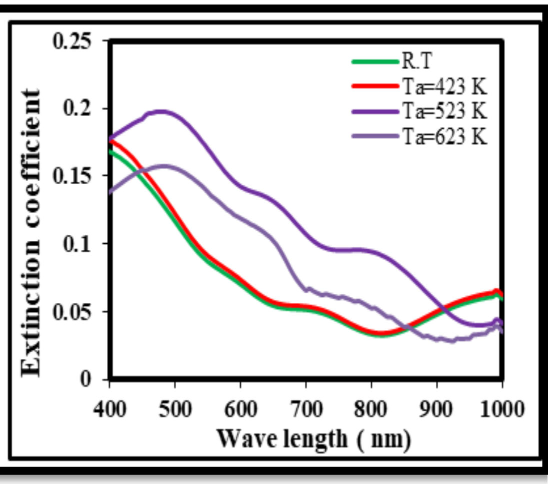

Figure 5. Refractive index contrasted with length for CZS thin films divers annealed temperature.

Figure 6. Extinction coefficient versus wave For CZS thin films divers annealed temperature.

The loss tangent (tanδ) for $Cu_{0.75}Zn_{0.25}S$ thin films by way of purpose for annealed temperatures **Figure 7** is evaluated from equation (10) which mainly depends on real (εr) and imaginary εi parts of the dielectric constant and denotes the characteristic debauchery of electromagnetic energy in the material into heat. This figure shows the loss factor (tanδ) values differ through wavelength from (0.01) to (0.35) contingent on grain size, structural defects, and lattice strain in the films.

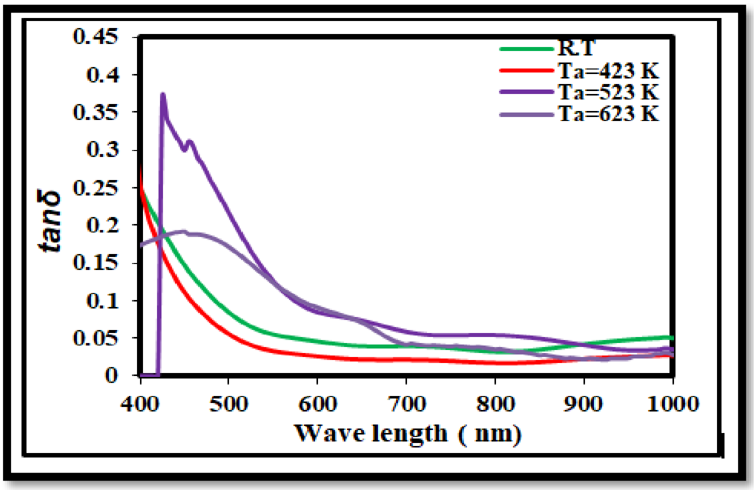

Figure 7. Variation loss tangent with wavelength for $Cu_{0.75}Zn_{0.25}S$ thin films before and after annealing.

4. Conclusions

In this work, the possibility of preparing $Cu_{0.75}Zn_{0.25}S$ Nanocrystalline thin films with 450 nm thickness using the thermal evaporation method is deposited on a glass substrate before and after annealing at (423,523,623) K for one hour. The crystal structure of $Cu_{0.75}Zn_{0.25}S$ films from the XRD study confirms that these films have mixed phases of CuS and ZnS and are polycrystalline hexagonal with preferential orientation along the (102) plane, and when increasing annealing temperatures caused enhanced film structures, the crystallite size increased and there was a small displacement in the spectrum curve towards high values of angle diffraction. The atomic force microscope (AFM) results show uniform distribution, and the annealing temperatures played an essential role in the grain size, which increased after annealing. Optical measurement results confirm the nature of electronic transitions for $Cu_{0.75}Zn_{0.25}S$ films was allowed direct transition electronic, the absorbance values increased after annealing, the CZS thin films have high values of absorption coefficient, and the direct energy gap (Eg) decreased from 2.3 eV to 1.8 eV with increase annealing temperatures, which decreased towards the mid of the visible region, which makes $Cu_{0.75}Zn_{0.25}S$ films suitable for photovoltaic application.

Acknowledgment

We thank the Thin Film Lab., Department of Physics, College of Education for Pure Science/ Ibn Al-Haitham, University of Baghdad.

Conflict of Interests

The authors declare that they have no conflicts of interest.

Funding

None.

Ethical Clearance

The project was approved by the local ethical committee at the University of Baghdad.

References

1. Sreejith MS. Tuning of properties of sprayed CuZnS films. AIP Conf Proc. 2014;1591:1741-3. https://doi.org/10.1063/1.4873096.
2. Edwin Jose MC, Santhosh K. Room temperature deposition of highly crystalline Cu-Zn-S thin films for solar cell applications using SILAR method. Journal of Alloys and Compounds. 2017;712:649-56. https://doi.org/10.1016/j.jallcom.2017.04.097.
3. Aabel P, Santhosh MC. A comprehensive review of the prospects for future hydrogen storage in materials-application and outstanding issues. Int J Energy Res. 2020;23(2):1–11. https://doi.org/10.1002/er.5227.
4. Wang H, Geng DY, Zhang YJ, Zhang ZD. CuS: Ni flowerlike morphologies synthesized by the solvothermal route. Mater Chem Phys. 2010;122:241–5. https://doi.org/10.1016/j.matchemphys.2010.02.042.
5. López MC. Growth of ZnS thin films obtained by chemical spray pyrolysis: The influence of precursors. J Cryst Growth. 2005;285:66-75. https://doi.org/10.1016/j.jcrysgro.2005.07.050.
6. Saranya M, Santhosh C, Ramachandran R, Kollu P, Saravanan P, Vinoba M. Hydrothermal growth of CuS nanostructures and its photocatalytic properties. Powder Technol. 2014;252(25):32-4. https://doi.org/10.1016/j.powtec.2013.10.031.
7. Abd El-Gawad AHM, Khalil AAI, Gadallah AS. Influence of preparation conditions on the properties of silver-doped copper-zinc sulfide thin films prepared via sol-gel spin coating technique. Optik. 2020;223:165561. https://doi.org/10.1016/j.ijleo.2020.165561.
8. Nanasaheb P, Huse RM, Patil RS. Characterization of economic and non-toxic copper doped zinc sulfide thin film grown by facile chemical bath deposition method. ES Mater Manuf. 2023;20:839. https://doi.org/10.30919/esmm5f839.
9. Masaya I, Yosuke M. Conduction type of nonstoichiometric alloy semiconductor CuxZnyS deposited by the photochemical deposition method. Thin Solid Films. 2015;594:277–81. https://doi.org/10.1016/j.tsf.2015.04.071.
10. Heidari G. Application of CuSeZnS PN junction for photoelectrochemical water splitting. Int J Hydrogen Energy. 2017;42:9545–52. https://doi.org/10.1016/j.ijhydene.2017.01.176.
11. Wang X, Peng W, Li X. Photocatalytic hydrogen generation with simultaneous organic degradation by composite CdSeZnS nanoparticles under visible light. Int J Hydrogen Energy. 2014;39:13454–61. https://doi.org/10.1016/j.ijhydene.2014.04.034.
12. Thuy U, Liem N, Parlett C, Lalev G, Wilson K. Synthesis of CuS and CuS/ZnS core/shell nanocrystals for photocatalytic degradation of dyes under visible light. Catal Commun. 2014;44:62-7. https://doi.org/10.1016/j.catcom.2013.07.030.
13. Guan XH, Qu P, Guan X, Wang GS. Hydrothermal synthesis of hierarchical CuS/ZnS nanocomposites and their photocatalytic and microwave absorption properties. RSC Adv. 2014;4:15579–85. https://doi.org/10.1039/C4RA00659C.
14. Yu J, Zhang J, Liu S. Ion-exchange synthesis and enhanced visible-light photoactivity of CuS/ZnS nanocomposite hollow spheres. J Phys Chem C. 2010;114:13642–9. https://doi.org/10.1021/jp101816c.
15. Gubari GM, Ibrahim SM, Huse NP, Dive AS, Sharma R. An experimental and theoretical study of Cu0.2Zn0.8S thin film grown by facile chemical bath deposition as an efficient photosensor. J Electron Mater. 2018;47:6128–35. https://doi.org/10.1007/s11664-018-6491-3.
16. Diamond AM, Corbellini L, Balasubramaniam KR, Chen S, Wang S, Matthews TS, et al. Copper-alloyed ZnS as a p-type transparent conducting material. Phys Status Solidi. 2017;20(12):209–101https://doi.org/10.1002/pssa.201228181.
17. Yang K, Nakashima Y, Ichimura M. Electrochemical deposition of CuxS and CuxZnyS thin films with p-type conduction and photosensitivity. J Electrochem Soc. 2012;159:H250–H254. https://doi.org/10.1149/2.042203jes.
18. Man D, Kai Y, Ichimura M. Semiconductor. Sci Technol. 2012;27:125007. https://doi.org/10.1088/0268-1242.

19. Ichimura M, Maeda Y. Solid-State Electronics. 2015;107:8-10. https://doi.org/10.1016/j.sse.2015.02.016.
20. Ni WS, Lin YJ. A novel Ni/WOX/W resistive random access memory with excellent retention and low switching current. Appl Phys A. 2015;119:1127–32. https://doi.org/10.1007/s00339-015-9079-2.
21. Aabel P, Santhosh MC. Deposition and characterization of earth abundant CuZnS ternary thin films by vacuum spray pyrolysis and fabrication of p-CZS/n-AZO heterojunction solar cells. Int J Energy Res. 2020;23(12):1–11.
22. Adelifard M, Eshghi H, Bagheri MM. Synthesis and characterization of nanostructural CuS–ZnS binary compound thin films prepared by spray pyrolysis. Optics Commun. 2012;285:4400–4. https://doi.org/10.1016/j.optcom.2012.06.030.
23. Sreejith MS, Deepu DR, Kartha CS, Rajeevkumar K, Vijayakumar KP. Tuning the properties of sprayed CuZnS films for fabrication of solar cell. Appl Phys Lett. 2014;105:202107. https://doi.org/10.1063/1.4902224.
24. Yildirim MA. Phys E: Low Dimens Syst Nanostruct. 2009;41:1365–72. https://doi.org/10.1016/j.physe.2009.04.014.
25. Chen C, Shi JB, Wu C, Chen CJ, Lin YT, Wu PF. Fabrication and optical properties of CuS nanowires by sulfuring method. Mater Lett. 2008;62:1421. https://doi.org/10.1016/j.matlet.2007.08.076.
26. Abbas H, Al-Obeidi H, Bushra KH. Effect of thermal annealing on the structural and optical properties of Sb2Se3 thin films. AIP Conf Proc. 2023;2475:090026. https://doi.org/10.1063/5.0123128.
27. Duaa MS, Bushra KH. The effect of thickness on electrical conductivity and optical constant of Fe2O3 thin films. Ibn Al-Haitham J Pure Appl Sci. 2023;36(2):113–23. https://doi.org/10.30526/36.2.2930.
28. Hamid AA, Bushra KH. Synthesis and characterization of Cu2S:Al thin films for solar cell applications. Chalcogenide Lett. 2022;19(9):579–90. https://doi.org/10.15251/CL.2024.215.385.
29. Ghuzlan SA, Bushra KH. Opto-electrical properties of p-SnSe:S/N-Si heterojunction for solar cell application. AIP Conf Proc. 2019;2123:020074. https://doi.org/10.1063/1.5117001.
30. Athab RH, Hussein BH. Fabrication and study of characteristics of HgSr2Can-1CunOδ+10 (n = 1, 2, and 3) thin films superconducting. Digest J Nanomater Biostruct. 2022;17(4):1173–80. https://doi.org/10.15251/DJNB.2022.174.1173.
31. Bushra HH, Hanan KH. Study and preparation of optoelectronic properties of AgAl1-xInxSe2/Si heterojunction solar cell applications. NeuroQuantology. 2020;18(5):77–87. https://doi.org/10.14704/nq.2020.18.5.NQ20171.
32. Al-Maiyaly BKH, Hussein BH, Hassan HK. Growth and optoelectronic properties of p-CuO:Al/n-Si heterojunction. J Ovonic Res. 2020;16(5):267–71. https://chalcogen.ro/267_MaiyalyBKH.pdf.
33. Ali SM, Hassun HK, Salih AA, Athabb RH, Al-Maiyaly BK, Hussein BH. Study the properties of Cu2Se thin films for optoelectronic applications. Chalcogenide Lett. 2022;19(10):663–71. https://doi.org/10.15251/CL.2022.1910.663.
34. S. Sreekanth, K. Santhosh. Fabrication and characterization of Cu-Zn-S thin films for solar cell applications. Solar Energy Materials and Solar Cells**.** 2016,147: 136–142. https://doi.org/10.1016/j.solm
35. Ali AY, Aseel AJ. Structure, surface morphology and optical properties of CuxZn1-xS/Au NPs layer for photodetector application. Int J Innov Sci Eng Technol. 2015;2(34):12-23. https://doi.org/10.1088/1742-6596/1234/1/012012.
36. Radloff GH, Naba FM, Ocran S, Bennett ME, Sterzinger KM, Armstrong AT.Fabrication and characterization of highly efficient dye-sensitized solar cells with composited dyes. Digest J Nanomater Biostruct. 2022;17(2):457-72. https://doi.org/10.15251/DJNB.2022.172.457.
37. Ali Yildirim MA, Aytunc At, Aykut A. Annealing and light effect on structural, optical and electrical properties of CuS, CuZnS and ZnS thin films grown by the SILAR method. Phys E. 2009;41(2):1365–72. https://doi.org/10.1016/j.physe.2009.04.014.